Electrochemical properties and corrosion protection of organosilane self-assembled monolayers on aluminum 2024-T3

Paul E. Hintze [a,b], Luz Marina Calle [b,*]

[a] National Research Council Resident Research Associate, ASRC-15, Kennedy Space Center, FL 32899, USA
[b] NASA Kennedy Space Center, YA-C2-T, Kennedy Space Center, FL 32899, USA

Abstract

Aluminum 2024-T3 surfaces were modified by the deposition of organosilane self-assembled monolayers (SAMs) and studied by surface characterization and electrochemical measurements. The SAMs were hydrophobic and had infrared spectral trends consistent with a densely packed hydrocarbon SAM. Electrochemical testing indicated that anodic dissolution was suppressed on the SAM modified surfaces while cathodic reduction of oxygen was not. Polarization resistance and capacitance values from EIS measurements were used to evaluate the corrosion protection of the SAMs. On exposure to 0.5 M NaCl, the polarization resistance values of the SAM modified surfaces quickly converge to values similar to the bare surface even though the capacitance values indicate the continued presence of the SAM. There are a large number of defects on SAM modified 2024-T3 relative to SAMs on pure substrates. The defects probably occur over copper enriched particles found on the 2024-T3 surface. The copper enriched particles must be protected by a coating since localized corrosion originates on the particles.

1. Introduction

Self-assembled monolayers (SAMs) are becoming a common form of surface modification. SAMs have been investigated for their properties of corrosion protection [1–5], anti microbial applications [6] and adhesion [5]. SAMs achieve their properties in a very efficient manner. A SAM forms an organized surface that can be made to expose a specific functionality of the molecule, e.g. hydrocarbon or amine. This makes SAMs ideal for changing surface properties. A small number of total molecules can profoundly impact the surface properties of a material.

Pioneering work on SAM properties has been mostly carried out on pure, relatively homogeneous surfaces, such as gold [7,8], aluminum [9,10], silicon and other semiconductors, [11,12] and glass [12,13]. More recently, studies of SAMs as corrosion protectors on iron [1–4,14], copper [5,15] and aluminum [16] have been reported. In each of these cases, however, relatively pure (>99.9% purity) metal substrates were used.

The use of SAMs on an alloy is a natural extension of this field. A SAM can be used as a model system of bonding to a surface, in this case revealing insight about the bonding of bulk siloxane polymers to aluminum alloy surfaces. An alloy surface tends to be considerably more inhomogeneous than a pure metal surface. Copper rich alloys, like Al 2024-T3, tend to undergo localized corrosion at copper rich particles [17]. The copper rich particle acts as cathode in a galvanic couple between it and the aluminum matrix. Effective protection of the particles will prevent the cathodic reaction therefore preventing localized corrosion.

The objective of this work is to investigate the electrochemical properties and corrosion protection properties of organosilane SAMs on aluminum alloy 2024-T3. This work involved the evaluation of the corrosion protection properties

* Corresponding author.
E-mail address: Luz.M.Calle@nasa.gov (L.M. Calle).

of SAMs formed from *n*-decyltriethoxysilane (DS) and *n*-octadecyltriethoxysilane (ODS) on aluminum alloy 2024-T3. Surface analysis methods as well as electrochemical measurements were used for this purpose.

2. Experimental

2.1. Preparation of SAMs

N-Decyltriethoxysilane, $CH_3(CH_2)_9Si(OCH_2CH_3)_3$, (>95%) (DS) and *n*-octadecyltriethoxysilane, $CH_3(CH_2)_{17}Si(OCH_2CH_3)_3$, (>95%) (ODS) were obtained from Gelest Inc., Morrisville, PA, and used without further purification. All other reagents were reagent grade. Aluminum alloy 2024-T3 was purchased from ACT Laboratories, Hillsdale, MI. The 2024-T3 samples were polished with 800 grit sand paper. The polished samples were cleaned in a sonicator, dried and then dipped briefly (10–15 s) in concentrated nitric acid. The metal samples were stored in an oven between cleaning and coating to prevent their contamination by atmospheric carbon.

The formation of a silane SAM on an oxide surface occurs in two steps, conversion to a silanol followed by condensation on the surface. Ethoxy silanes ($R_3SiOCH_2CH_3$) must be converted to silanols (R_3SiOH) before SAM formation. The ethoxy silanes were hydrolyzed to silanols in a solution of 0.02 M silane, 0.006 M HCl and 0.28 M H_2O in ethanol. This solution sat for 4 h to allow for hydrolysis. The hydrolysis solution was then diluted by a factor of 10 and the alloy immersed in this solution for 10 min. The silanol undergoes a condensation reaction with a hydroxide group on the alloy surface forming the siloxane linkage (metal–O–Si). Following immersion, the SAMs were cured in a 50 °C oven overnight. This SAM deposition procedure was selected after trying different concentrations of silanes, different solvents and different immersion times. Using water contact angle measurements as a relative gauge of SAM quality or coverage (larger contact angles and lower hysteresis indicating more complete coverage by the SAM [18,19]), these conditions were found to provide the best SAM in the shortest amount of time and with a non-hazardous solvent, ethanol. No enhancement of the contact angle was gained for samples immersed in this solution overnight or for SAMs deposited from other solutions.

2.2. Surface characterization

The coated and bare surfaces were characterized by dynamic contact angle measurements, Fourier transform infra-red (FTIR) spectroscopy, scanning electron microscopy (SEM), equipped with an energy dispersive spectroscopy (EDS) detector and X-ray photoelectron spectroscopy (XPS). Water contact angle measurements were made with a Cahn DCA-312 dynamic contact angle analyzer. The DCA-312 employs a Wilhelmy plate method where a sample is slowly lowered into and raised from a reservoir of water while the force on the sample is measured by a balance. The contact angle, θ, is calculated from the equation, $\cos\theta = F \times g/ST \times P$, where F is the force on the sample at zero immersion depth, g the acceleration due to gravity, ST the surface tension of water and P is the perimeter of the sample at the interface [20]. FTIR spectra were measured using a Nicolet Magna IR 760 spectrophotometer equipped with a Spectra Physics 80° grazing angle accessory using a $4\,cm^{-1}$ spectral resolution. A JEOL JSM 5900LV SEM was used to characterize the polished metal. XPS measurements were made with a Kratos XSAM800.

2.3. Electrochemical evaluation

All electrochemical measurements were performed with a Princeton Applied Research PARSTAT 2263 potentiostat. The electrolyte was a 0.5 M solution of NaCl. Values reported later in the text are the average of at least three separate measurements. Potentiodynamic scans were done in an electrochemical cell with a $1\,cm^2$ exposed area of working electrode, a platinum mesh counter electrode and a standard calomel electrode (SCE) as reference. The potentiodynamic scans were done after the electrode had been exposed to the 0.5 M NaCl solution with air bubbling through it for 30 min. The scans were done from 100 mV below to 150 mV above the open circuit potential.

EIS measurements were made from 100 kHz to 10 mHz with a 5 mV amplitude. The test cells employed a $13\,cm^2$ working electrode, a platinum mesh counter electrode and an SCE reference electrode. EIS measurements were obtained under either a nitrogen (N_2) atmosphere or with air bubbled through the electrolyte. For testing under an N_2 atmosphere, N_2 was bubbled through the electrolyte before the start of the EIS data collection, and then blown through the head space of the electrochemical cell.

3. Results and discussion

3.1. Surface characterization

The advancing, θ_a, and receding, θ_r, water contact angles are shown in Table 1. As expected, modification of the surfaces with the hydrophobic silane SAMs leads to a much

Table 1
Advancing and receding water contact angles, in degrees, and contact angle hysteresis ($\cos\theta_r - \cos\theta_a$) for bare, DS and ODS modified Al 2024-T3 surfaces

	Advancing water contact angle/degrees	Receding water contact angle/degrees	Water contact angle hysteresis
Bare	51° (5°)	10° (3°)	0.6
DS	117° (23°)	49° (29°)	1.1
ODS	113° (11°)	61° (22°)	0.9

Standard deviations for the measurements are given in parenthesis.

larger contact angle. Care should be taken in comparing measured contact angles, as different measurement techniques can produce different absolute values for the angles. The angles reported here are dynamic contact angles and may be different from static angles, although relative trends will be the same. The advancing water contact angles were found to be larger than those reported in the literature for hydrocarbon monolayers on a variety of surfaces [3,4,8,9,19,21]. The hysteresis, defined as $\cos\theta_r - \cos\theta_a$, can be interpreted as a measure of the chemical and physical homogeneity of the surface. A small hysteresis is characteristic of a complete and homogeneous SAM, while a large hysteresis is associated with a degraded or incomplete layer [18,19]. The hysteresis values reported here are larger by at least an order of magnitude than values reported for other hydrocarbon SAMs on gold [8] and silicon [19]. The large hysteresis values appear to be due to the substrate, not the SAM deposition procedure. Hysteresis values of less than 0.05 were consistently obtained when a glass microscope slide was used instead of the aluminum 2024-T3 panel with the same SAM solution. In addition, while optimizing the SAM deposition procedure, θ_a did not vary by much while θ_r varied widely. This suggests that θ_r is a sensitive measure of SAM quality. The large hysteresis on the Al 2024-T3 surface suggests that only a partial monolayer is formed.

FTIR spectra between 2800 and 3000 cm^{-1} for the bare, DS and ODS modified Al 2024-T3 surfaces are shown in Fig. 1. The peaks in the spectrum correspond to the carbon-hydrogen bond stretching vibrations. The high energy peak, $\sim$2960 cm^{-1}, corresponds to the terminal CH$_3$ stretching vibration while the other two peaks, $\sim$2920 cm^{-1} and $\sim$2850 cm^{-1}, are stretches in the –CH$_2$– backbone [7]. The intensity of the CH$_3$ peak is the same for both DS and ODS surfaces while the intensity of the CH$_2$ peaks is larger in ODS than in DS. This is consistent with expectations that no more than a monolayer is being formed. Each molecule of ODS and DS has one CH$_3$ group, so the intensity of that peak would be expected to remain constant if the number of molecules were
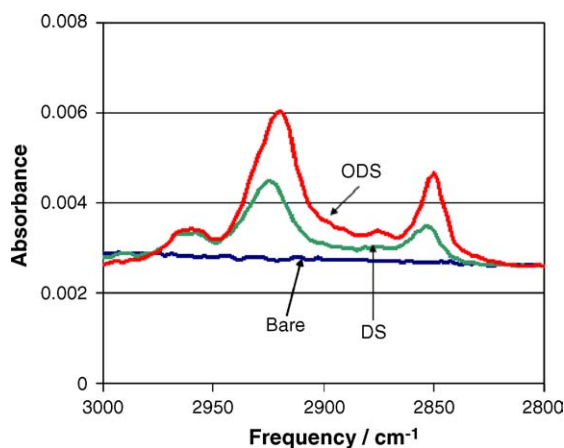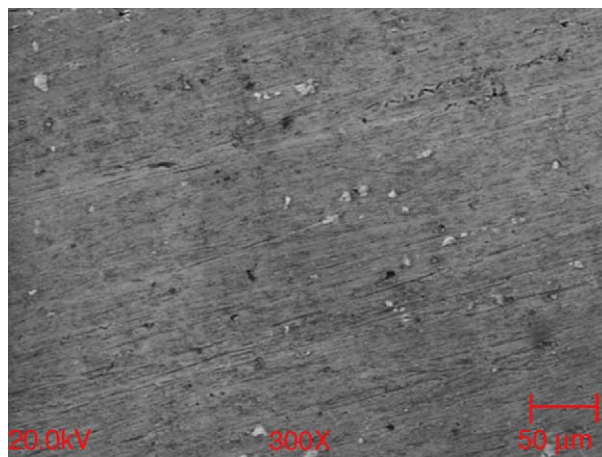
Fig. 2. An SEM micrograph of polished Al 2024-T3. The light spots are copper enriched particles.

the same. The CH$_2$ intensity should increase in the ODS surface since there is a longer backbone, and therefore more CH$_2$ groups, in that molecule. The maxima of the two CH$_2$ peaks are shifted to a lower frequency in the ODS SAM relative to the DS SAM. This has been associated with closer packing of hydrocarbon monolayers [7] from a comparison of crystalline and liquid hydrocarbons. Packing density is expected to increase with chain length. It was concluded from these results that both DS and ODS form monolayers with approximately the same coverage and that the ODS SAM is more tightly packed than the DS SAM.

Fig. 2 shows an SEM image of the bare Al 2024-T3 surface. EDS analysis indicates that the bright spots are copper enriched particles. The chemical state and large number of these particles could influence SAM formation. The silane SAM will only form on an oxide surface, therefore, if there is no oxide layer on the particles, the SAM will not form in that area.

3.2. Electrochemical evaluation

Potentiodynamic scans were performed to help identify the mechanisms of corrosion protection. Results are shown in Fig. 3. The E_{corr} values (-586 mV for the bare surface, -566 mV for the DS SAM and -557 mV for the ODS SAM) for the modified surfaces are shifted to more positive potentials with respect to the bare surface. These values are similar to shifts found on other systems [1,3]. Upon cathodic polarization, there is little difference between the coated and bare surfaces in contrast to what has been reported previously [2,3]. In those studies of alkanethiol monolayers on iron, the authors found that the monolayer inhibited the cathodic process and concluded that O$_2$ diffusion to the metal surface was suppressed. The similarity between the bare and coated surfaces under cathodic polarization indicates that the DS and ODS SAMs on Al 2024-T3 do not prevent O$_2$ diffusion to the surface in any significant way. This could be caused by two factors: (1) DS and ODS form SAMs over the entire Al

Fig. 1. Infrared spectrum of the C–H bond stretching region, 3000–2800 cm^{-1}, of bare, DS and ODS modified Al 2024-T3.
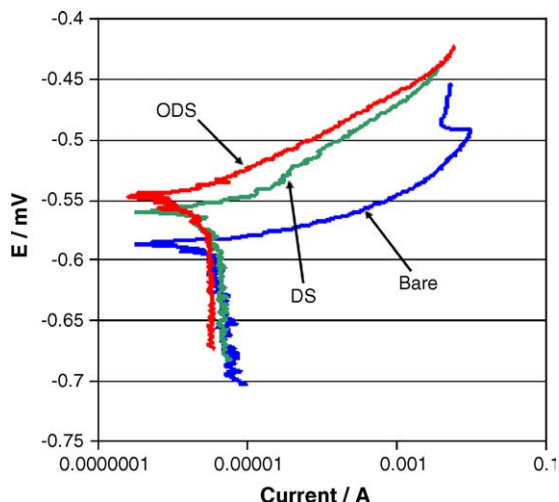
Fig. 3. Potentiodynamic scans of bare, DS and ODS modified Al 2024-T3 in 0.5 M NaCl.

2024-T3 surface, but the SAMs are not good quality densely packed barrier layers, or (2) locally, the DS and ODS SAMs are densely packed, but it is not a complete monolayer. The FTIR results indicated that the monolayers undergo typical trends in packing as chain length increases, suggesting that, at least locally, the molecules in the SAM are densely packed. In addition, the θ_a values are consistent with a well oriented, densely packed SAM. Therefore, it was concluded that the SAM is well ordered and closely packed over portions of the surface. It is likely that the surface is not covered by a complete monolayer and has a much greater number of defect sites than was found for SAMs on other surfaces. Since a silane will only bond to an oxide surface, the SAM may not form over the copper enriched particles if the particles are not covered by an oxide. Seegmiller and Buttry [22] showed that a higher redox activity was found over copper enriched particles relative to the matrix oxide surface, indicating that the cathodic reaction should occur mainly on the copper enriched particles. The similarity in cathodic behavior between SAM modified and bare surfaces, supports the conclusion that there is no SAM over the copper enriched particles. If these sites were in fact left open, a suppression of the cathodic current would not be expected.

The slope of the anodic I versus E curve is less for the SAM modified surface than for the bare surface. Therefore, the anodic current is moderately suppressed on the SAM modified surfaces. The suppression of anodic dissolution by SAMs is apparently very system specific. Previous measurements of alkanethiols SAMs on iron [2,3] and copper [15] found little or no change in anodic currents, while SAMs of phosphonoalkanes on iron [1] had markedly decreased anodic currents. These different results are possibly a consequence of the SAM bonding to the surface. SAMs attached by phosphono or silane groups bond to the oxide surface while thiols bond to the metallic surface.

EIS measurements were performed to investigate the electrochemical properties of the modified surface. Previous stud-

ies [1,3,23] have found a few characteristic effects in the electrochemical properties of a surface after being modified with a self-assembled monolayer. Changes in the double layer capacitance and interfacial capacitance have been found to correlate to SAM formation. The capacitance should decrease as the SAM coverage increases, since the capacitance is inversely proportional to the distance between the charges. In addition, the polarization resistance, which corresponds to the charge transfer resistance in the pores of the monolayer or bare surface, increases as the coverage increases.

Typical EIS spectra immediately after exposure to the electrolyte are shown in Fig. 4. The Bode plots of phase angle and impedance versus frequency show characteristic differences between the SAM modified and bare surfaces. Both SAM modified surfaces have a larger impedance and a quicker increase in phase angle than the bare surface. These changes are associated with the SAM. After 60 min, the spectra for the SAMs and bare surfaces are qualitatively the same as shown in Fig. 5. The Bode plots of impedance versus frequency are nearly the same while the phase angle plots still have some differences. As exposure time increases, the spectra remain qualitatively the same, each beginning to show signs of a diffusional impedance at low frequencies. The diffusional impedance has been associated with localized corrosion in this alloy [24].

Two approaches were taken to analyze the EIS data. The first involved looking at values found directly from the impedance spectra and the second involved equivalent circuit modeling.
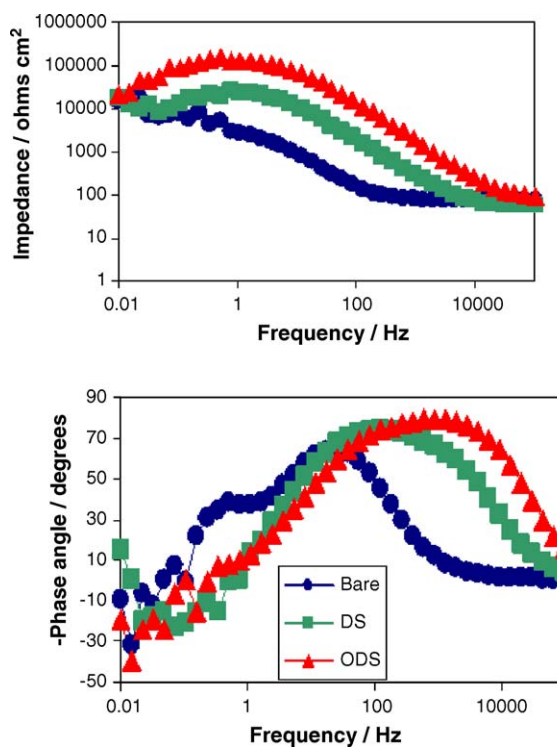
Fig. 4. Bode plots of bare, DS and ODS modified Al 2024-T3 in aerated 0.5 M NaCl immediately after exposure to the electrolyte.
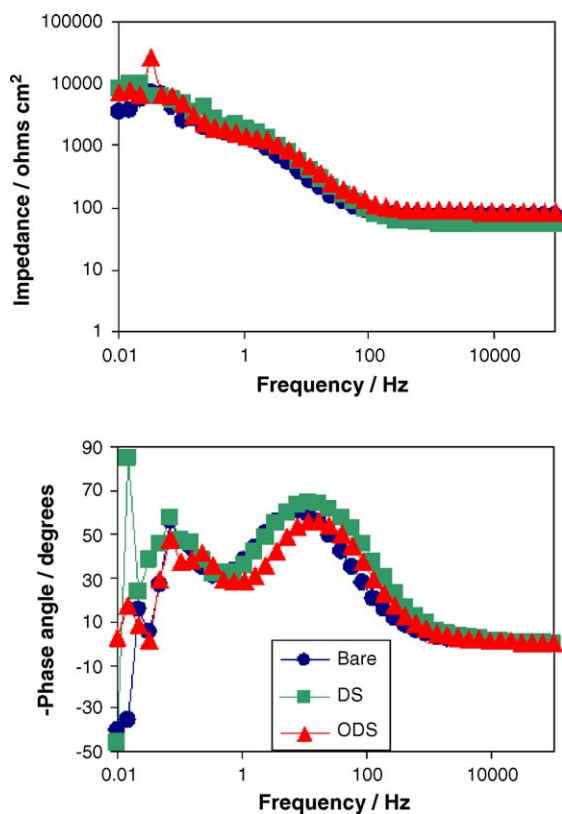
Fig. 5. Bode plots of bare, DS and ODS modified Al 2024-T3 in aerated 0.5 M NaCl after 1 h of exposure to the electrolyte.

The interfacial capacitance was measured from the 1.32 kHz point in each impedance spectra. Fig. 6 shows the average values of the measured interfacial capacitances of the samples in aerated 0.5 M NaCl over time. Immediately after immersion, the capacitance for the modified surfaces is lower by about a factor of 10 relative to the bare surface. After 2 h of exposure, the average capacitance values are not significantly different as the values are within 1 standard deviation of each other. This is true for both aerated and deaerated conditions. The interfacial capacitance, C_i, is influenced by the double
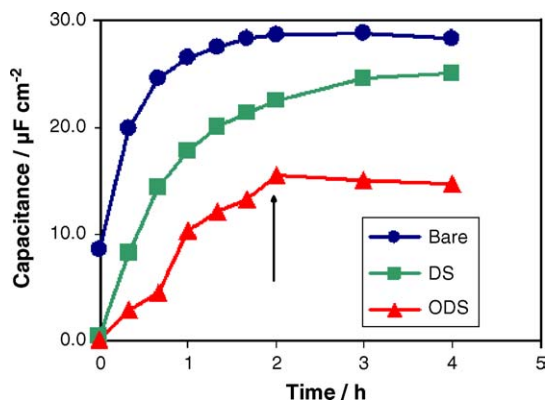
Fig. 6. Interfacial capacitance over time of bare, DS and ODS modified Al 2024-T3 in aerated 0.5 M NaCl measured at 1.32 kHz. The arrow indicates the time at which the standard deviations of the measurements all overlap.
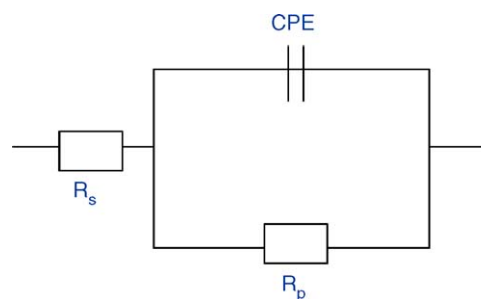
Fig. 7. The equivalent circuit used to model the high frequency EIS data. R_s is the solution resistance, R_p is the polarization resistance and CPE is a constant phase element.

layer capacitance, C_{dl}, of the bare surface and the capacitance of the SAM, C_{SAM}. If the fraction of SAM coverage is f, the interfacial capacitance of the surface is related to the individual capacitances by $C_i = (1 - f)C_{dl} + fC_{SAM}$. Since the double layer capacitance is larger than the capacitance of the SAM, it will dominate the total capacitance as the SAM coverage decreases. Therefore, the interfacial capacitances of SAM modified and bare surfaces can become similar even though there is still some SAM coverage on the surface. In fact, XPS confirms the continued presence of some silane molecules after 3 days of exposure to an aerated 0.5 M NaCl solution.

The high frequency EIS data was modeled with a Randle's circuit modified with a constant phase element (CPE) in place of the capacitor as shown in Fig. 7. The impedance of a CPE depends on the frequency via the equation $Z_{CPE} = 1/C(j\omega)^n$ where C is the capacitance. As n approaches 1, the impedance of a CPE reduces to that of a true capacitor. The R_p values in aerated 0.5 M NaCl are shown in Fig. 8. After initial immersion, the R_p values for the SAM modified surfaces are larger than the bare surface indicating that the charge transfer resistance is increased. After just 20 min, the R_p values are within a standard deviation of each other in both aerated and deaerated conditions. The SAM no longer acts as a barrier to redox reactions after a very short time (Fig. 9).
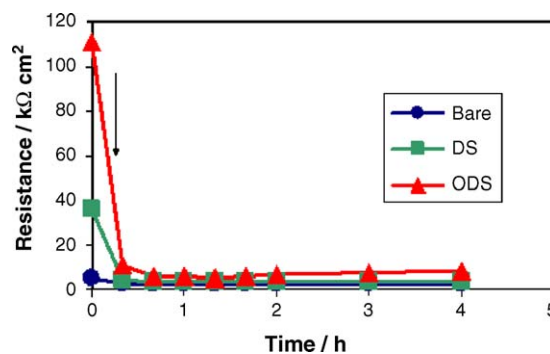
Fig. 8. R_p values, calculated using the equivalent circuit in Fig. 7, over time of bare, DS and ODS modified Al 2024-T3 in aerated 0.5 M NaCl. The arrow indicates the time at which the standard deviations of the measurements all overlap.
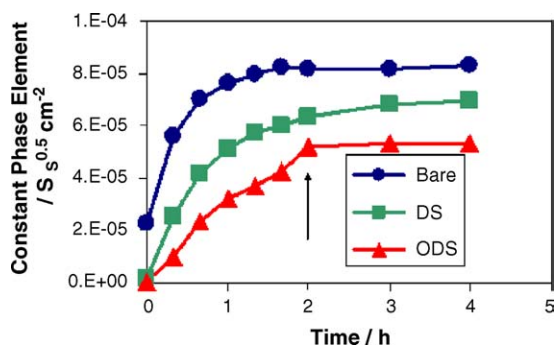
Fig. 9. CPE values, calculated using the equivalent circuit in Fig. 7, over time of bare, DS and ODS modified Al 2024-T3 in aerated 0.5 M NaCl. The arrow indicates the time at which the standard deviations of the measurements all overlap.

The CPE value behaves in the same way as the interfacial capacitance. Initially the CPE is lower for the modified surfaces and after 2 h the average values are within one standard deviation of each other. The n values of the CPE are within one standard deviation of each other after 2 h in aerated solutions. However, the n values are significantly different even after 20 h in the deaerated solution. The difference between aerated and deaerated solutions might be caused by the more rapid formation of corrosion products in the aerated solution.

The EIS data is consistent with a SAM surface that has a large number of defects. Immediately after exposure begins, the SAM surface behaves as a barrier to redox activity as evidenced by larger R_p values. However, the barrier effect disappears very quickly as shown by the converging R_p values for SAM modified and bare surfaces. The capacitance values, both interfacial and modeled with an equivalent circuit, are affected by the SAM for longer periods of time than the R_p values. If the redox activity occurs mostly on the copper enriched particles of Al 2024-T3 [22], and these particles are not covered by the SAM, then these results are what would be expected.

4. Conclusions

Organosilanes form SAMs with a large number of defects on Al 2024-T3. Although there is good coverage on the aluminum oxide surface, the defects are probably centered on copper enriched particles, which are distributed throughout the alloy surface. Electrochemical measurements suggest that the SAM modified surfaces do not provide a great deal of protection from localized corrosion because the copper rich particles are not protected. This behavior can be expected on any surface that does not have a homogeneous surface oxide layer.

It is suggested that the copper enriched particles must be protected in order for SAM modification to provide significant corrosion protection on 2024-T3 surfaces. This can be

achieved by applying a monolayer that bonds to both the particles and oxide surface, applying a mixed monolayer or by devising surface preparation techniques that induce more complete SAM coverage. This study of bonding to the Al 2024-T3 surface should aid in the development of coatings that are more efficient and can be used as replacements for chromate conversion coatings.

Acknowledgements

References

[1] I. Felhosi, J. Telegdi, G. Palinkas, E. Kalman, Electrochim. Acta 47 (2002) 2335.
[2] K. Nozawa, H. Nishihara, K. Aramaki, Corros. Sci. 39 (1997) 1625.
[3] K. Nozawa, K. Aramaki, Corros. Sci. 41 (1999) 57.
[4] K. Aramaki, T. Shimura, Corros. Sci. 46 (2004) 313.
[5] C.M. Whelan, M. Kinsella, H.M. Ho, K. Maex, J. Electrochem. Soc. 151 (2004) 33.
[6] S. Jon, J. Seong, A. Khademhosseini, T.-N.T. Tran, P.E. Laibinis, R. Langer, Langmuir 19 (2003) 9989.
[7] M.D. Porter, T.B. Bright, D.L. Allara, C.E.D. Chidsey, J. Am. Chem. Soc. 109 (1987) 3559.
[8] C.D. Bain, E.B. Troughton, Y.-T. Tao, J. Evall, G.M. Whitesides, R.G. Nuzzo, J. Am. Chem. Soc. 111 (1989) 321.
[9] D.L. Allara, R.G. Nuzzo, Langmuir 1 (1985) 45.
[10] D.L. Allara, R.G. Nuzzo, Langmuir 1 (1985) 52.
[11] I. Haller, J. Am. Chem. Soc. 100 (1978) 8050.
[12] R. Maoz, J. Sagiv, J. Colloid Interface Sci. 100 (1984) 465.
[13] J. Sagiv, J. Am. Chem. Soc. 102 (1980) 92.
[14] I. Felhosi, J. Telegdi, K. Papp, E. Kalman, A. Stahl, J. Bognar, Macromol. Sym. 187 (2002) 305.
[15] M. Itoh, H. Nishihara, K. Aramaki, J. Electrochem. Soc. 141 (1994) 2018.
[16] M.A. Petrunin, A.P. Nazarov, Y.N. Mikhailovski, J. Electrochem. Soc. 143 (1996) 251.
[17] R.G. Buchheit, R.P. Grant, P.F. Hlava, B. Mckenzie, G.L. Zender, J. Electrochem. Soc. 144 (1997) 2621.
[18] K. Efimenko, B. Novick, R.G. Carbonell, J.M. DeSimone, J. Genzer, Langmuir 18 (2002) 6170.
[19] J.B. Brzoska, I. Ben Azouz, F. Rondelez, Langmuir 10 (1994) 4367.
[20] I. Cahn Instruments DCA-312 Instruction Manual, 1991.
[21] J. Peanasky, H.M. Schneider, S. Granick, Langmuir 11 (1995) 953.
[22] J.C. Seegmiller, D.A. Buttry, J. Electrochem. Soc. 150 (2003) 413.
[23] R.D. Weinstein, J. Moriarty, E. Cushnie, R. Colorado Jr., T.R. Lee, M. Patel, W.R. Alesi, G.K. Jennings, J. Phys. Chem. B 107 (2003) 11626.
[24] F. Mansfeld, Y. Wang, S.H. Lin, H. Xiao, H. Shih, Detection and monitoring of localized corrosion by EIS, in: J.R. Scully, D.C. Silverman, M.W. Kendig (Eds.), Electrochemical Impedance: Analysis and Interpretation, ASTM STP 1188, ASTM, Philadelphia, PA, USA/San Diego, CA, USA, 1993, p. 297.